

Adaptive Alignment for Low-Cost INS in ECEF Frame Under Large Initial Attitude Errors

Kedong Wang¹ | Wei Gao¹ | Xiaohan Xu¹ | Jinling Wang²

¹ School of Astronautics, Beihang University, Beijing 100191, China

² School of Civil and Environmental Engineering, UNSW Australia, Sydney, NSW 2052, Australia

Correspondence

Kedong Wang
School of Astronautics
Beihang University
Beijing 100191, China
Email: wangkd@buaa.edu.cn

Abstract

A new two-stage alignment on a moving base is proposed for a low-cost inertial navigation system with the aid of a Global Positioning System (GPS) receiver in the Earth-centered, Earth-fixed (ECEF) frame under large initial attitude errors. Both the state and measurement equations are derived using the additive quaternion error model in the ECEF frame for alignment without the need for level adjustment. The nonlinear velocity error equations in both the coarse and the fine stages are linearized further. An improved strong tracking filter is proposed for the coarse stage to converge quickly with large initial attitude errors. After the attitude errors converge to smaller values in the coarse stage, a standard Kalman filter is implemented for the fine stage. Experiments demonstrate that attitude error can converge quickly with the proposed adaptive alignment method.

Keywords

alignment, GPS, inertial navigation system, Kalman filter

1 | INTRODUCTION

Although low-cost inertial measurement unit (IMU) sensors, such as micro-electromechanical systems (MEMS), accelerometers, and gyroscopes, have improved significantly in accuracy, an inertial navigation system (INS) composed of low-cost IMU sensors is still difficult to align accurately with stationary self-alignment (Li & Wang, 2012; Syed et al., 2008). However, if it is aided by global navigation satellite system (GNSS) measurements on a moving base, it may be aligned accurately and quickly (Kaygisiz & Şen, 2014; Tsukerman & Klein, 2018; Wu & Pan, 2013; Zhong et al., 2018).

An in-motion alignment algorithm based on optimization called the *Optimization-Based Alignment* (OBA) that converges very quickly in the coarse stage has been put forward to estimate the three attitude angles, IMU sensor biases, and even the GNSS antenna's level arm recursively (Chang et al., 2016; Chen et al., 2021; Wu et al., 2014; Wu & Pan, 2013). Unfortunately, neither the states nor their covariances of the Kalman filter (KF) in the fine stage can be initialized by the OBA directly. Instead, if the alignment in the coarse stage is implemented by a KF, the KF in the fine stage can be conveniently initialized by the converged results in the coarse stage. In the coarse stage, the main challenge faced by the KF is the

nonlinear state equations, which have been studied intensively (Kaygisiz & Şen, 2014; Li & Wang, 2012; Tsukerman & Klein, 2018; Zhong et al., 2018).

If a stationary level adjustment is accomplished before the initial alignment in the local level frame, both the pitch and the rolling errors would be small, but the yaw error would still be very large for the low-cost INS. That is, in the local level frame, the in-motion alignment in the coarse stage would still suffer the severe nonlinearity in the filtering model (Syed et al., 2008). Unscented Kalman filters (UKFs) and other nonlinear filters have been proposed for coarse alignment (Dmitriyev et al., 1997; Kong et al., 1999; Shin & El-Sheimy, 2004), but they exhaust more computational loads than a linear KF.

The state equations in the wander yaw frame will be linear if the cosine and sine values of the yaw error, rather than the yaw error itself, are included in the states (Han & Wang, 2010; Pham, 1991; Qi & Pengfei, 2015; Rogers, 1997). Unfortunately, both the states and the state equations in the fine stage are different from those with the sine and cosine terms in the coarse stage, so the filtering results in the coarse stage cannot be employed to initialize the filter in the fine stage directly. Alternatively, if the state equations in the two stages are derived by the quaternion method, the states in the fine stage will be the same as those in the coarse stage. In fact, the state equations without the assumption of small attitude errors have been derived using the linear Additive Quaternion Error (AQE) model (Yu et al., 1997, 1999). However, the velocity error equations derived using the AQE model are nonlinear for the large yaw error even though the level adjustment has been accomplished before the coarse stage. Hence, they will have to be linearized for the linear KF, but the linearization error in the coarse stage will be very large, which is not beneficial in improving alignment performance.

The linearized velocity error equations using the AQE model have been elaborated to further improve on alignment performance (Wang et al., 2020). Moreover, if the fading KF is used to improve the contribution of the latest measurements in the state updating (Geng & Wang, 2008; Simon, 2006), the impact of the linearized error on alignment can be mitigated significantly. Considering that the fading factor is usually preset as a constant, a strong tracking filter (STF) has been employed to adjust the fading factor adaptively by the updated residual (Zhong et al., 2018). Consequently, all the states are attenuated by the fading factor equally in both the fading KF and the STF. However, by using the AQE model, both the attitude error and the position error equations are linear, while only the velocity error equations are nonlinear. Hence, it is more reasonable to allocate the states with different fading factors to address the difference among the state equations, which has yet to be investigated until now.

If the INS navigation is implemented in the Earth-centered, Earth-fixed (ECEF) frame, rather than in the local level frame, more than 30% of the computational load can be reduced, which is attractive to low-cost applications because of the limited online computation (Wei & Schwarz, 1990). Correspondingly, the INS should be initially aligned in the ECEF frame, too. Actually, linearized alignment in the ECEF frame has been proposed, but it is derived by assuming small attitude errors (Xie et al., 2014). Furthermore, the level adjustment in the local level frame will lose its effectiveness for alignment in the ECEF frame. That is, alignment in the ECEF frame should be implemented with the condition of large attitude errors rather than only one large yaw error, which has not been studied either.

In this paper, a new two-stage alignment on a moving base is proposed for a low-cost MEMS INS with the aid of a Global Positioning System (GPS) receiver in the ECEF frame under large initial attitude errors. Both the state and measurement equations are derived in the ECEF frame for alignment without the need for

a level adjustment. The nonlinear velocity error equations are linearized in both the coarse and fine stages further. An improved STF algorithm is proposed for the coarse stage to converge quickly with large attitude errors. After the attitude errors converge to the small values in the coarse stage, a standard KF is implemented in the fine stage.

The rest of this paper is organized as follows. The AQE models in the ECEF frame are provided for the alignment on a moving base in Section 2. The velocity error equations are linearized for the following filtering. An improved STF is proposed for the coarse stage in Section 3. The proposed alignment is compared with those using a fading KF and an existing STF with a vehicle test to verify its performance in Section 4. Finally, conclusive remarks are provided for the proposed alignment's potential applications.

2 | STATE AND MEASUREMENT EQUATIONS USING THE AQE MODEL

The state equations, including the attitude error, velocity error, position error, and measurement equations, are derived using the AQE model in the ECEF frame. Nonlinear velocity error equations are linearized further in the following filtering.

2.1 | Attitude Error Equations

Herein, e and b represent the ECEF and body frames, respectively. The ECEF frame is assumed to be the navigation frame. Attitude errors are defined as the misalignment between the mathematical platform and the navigation frame. $\mathbf{q}_b^e = [q_0^e \ q_1^e \ q_2^e \ q_3^e]^T$ and $\tilde{\mathbf{q}}_b^e = [\tilde{q}_0^e \ \tilde{q}_1^e \ \tilde{q}_2^e \ \tilde{q}_3^e]^T$ are the true and indicated quaternion vectors, respectively. The AQE vector of \mathbf{q}_b^e and $\tilde{\mathbf{q}}_b^e$ is defined as:

$$\delta \mathbf{q}_b^e = \tilde{\mathbf{q}}_b^e - \mathbf{q}_b^e = [\delta q_0^e \ \delta q_1^e \ \delta q_2^e \ \delta q_3^e]^T \quad (1)$$

Then, the attitude error equations based on the AQE model are given as (Yu et al., 1999):

$$\delta \dot{\mathbf{q}}_b^e = \mathbf{M}^e \delta \mathbf{q}_b^e + \frac{1}{2} \mathbf{U}^e \delta \boldsymbol{\omega}_{ib}^b \quad (2)$$

where $\mathbf{M}^e = \frac{1}{2}(\tilde{\boldsymbol{\Omega}}_{ib}^b - \boldsymbol{\Omega}_{ie}^e)$, $\delta \boldsymbol{\omega}_{ib}^b = \tilde{\boldsymbol{\omega}}_{ib}^b - \boldsymbol{\omega}_{ib}^b$, $\boldsymbol{\omega}_{ib}^b = [\omega_{ibx}^b \ \omega_{iby}^b \ \omega_{ibz}^b]^T$ is the angular rate vector in the body frame, ω_{ie} equals 15.041°/h, and $\boldsymbol{\omega}_{ie}^e = [0 \ 0 \ \omega_{ie}^e]^T$ is the Earth rotation rate in the ECEF frame. Herein, the tildes indicate values with error. The other items are defined as:

$$\tilde{\boldsymbol{\Omega}}_{ib}^b = \begin{bmatrix} 0 & -\tilde{\omega}_{ibx}^b & -\tilde{\omega}_{iby}^b & -\tilde{\omega}_{ibz}^b \\ \tilde{\omega}_{ibx}^b & 0 & \tilde{\omega}_{ibz}^b & -\tilde{\omega}_{iby}^b \\ \tilde{\omega}_{iby}^b & -\tilde{\omega}_{ibz}^b & 0 & \tilde{\omega}_{ibx}^b \\ \tilde{\omega}_{ibz}^b & \tilde{\omega}_{iby}^b & -\tilde{\omega}_{ibx}^b & 0 \end{bmatrix} \quad (3)$$

$$\boldsymbol{\Omega}_{ie}^e = \begin{bmatrix} 0 & 0 & 0 & -\omega_{ie} \\ 0 & 0 & \omega_{ie} & 0 \\ 0 & -\omega_{ie} & 0 & 0 \\ \omega_{ie} & 0 & 0 & 0 \end{bmatrix} \quad (4)$$

$$\mathbf{U}^e = \begin{bmatrix} -\tilde{q}_1^e & -\tilde{q}_2^e & -\tilde{q}_3^e \\ \tilde{q}_0^e & -\tilde{q}_3^e & \tilde{q}_2^e \\ \tilde{q}_3^e & \tilde{q}_0^e & -\tilde{q}_1^e \\ -\tilde{q}_2^e & \tilde{q}_1^e & \tilde{q}_0^e \end{bmatrix} \quad (5)$$

Obviously, the attitude error equations in Equation (2) based on the AQE model are linear without any assumptions.

2.2 | Velocity Error Equations

The velocity equations in the ECEF frame are as follows:

$$\dot{\mathbf{v}}^e = \mathbf{f}^e - 2\boldsymbol{\omega}_{ie}^e \times \mathbf{v}^e + \mathbf{g}^e \quad (6)$$

where \mathbf{v}^e is the velocity vector in the ECEF frame; \mathbf{C}_b^e is the rotation matrix from the body frame to the ECEF frame; $\mathbf{f}^e = \mathbf{C}_b^e \mathbf{f}^b$, \mathbf{f}^e , and \mathbf{f}^b are the specific forces in the ECEF and the body frames, respectively; $\mathbf{a} \times$ is the skew-symmetric matrix of \mathbf{a} ; and \mathbf{g}^e is the gravity in the ECEF frame. The quaternions of the two 3D vectors, \mathbf{f}^e and \mathbf{f}^b , are denoted as $\mathbf{f}^{e'}$ and $\mathbf{f}^{b'}$, respectively. Their scalar and complex components are zero and 3D vectors, respectively. The specific force $\mathbf{f}^e = \mathbf{C}_b^e \mathbf{f}^b$ can be written as:

$$\mathbf{f}^{e'} = \mathbf{q}_b^e \circ \mathbf{f}^{b'} \circ \mathbf{q}_b^{e*} \quad (7)$$

where \circ denotes the quaternion multiplication and \mathbf{q}_b^{e*} is the complex conjugate of \mathbf{q}_b^e . The error of the specific force can be obtained as:

$$\delta \mathbf{f}^{e'} = \tilde{\mathbf{q}}_b^e \circ \tilde{\mathbf{f}}^{b'} \circ \tilde{\mathbf{q}}_b^{e*} - \mathbf{q}_b^e \circ \mathbf{f}^{b'} \circ \mathbf{q}_b^{e*} \quad (8)$$

where $\tilde{\mathbf{f}}^{b'}$ is the quaternion related to $\tilde{\mathbf{f}}^b$. If $\delta \mathbf{f}^e$ is the vector related to the quaternion $\delta \tilde{\mathbf{f}}^{e'}$, the velocity error equations can be derived as:

$$\delta \dot{\mathbf{v}}^e = \delta \mathbf{f}^e - 2\boldsymbol{\omega}_{ie}^e \times \delta \mathbf{v}^e + \delta \mathbf{g}^e \quad (9)$$

where $\delta \mathbf{v}^e$ and $\delta \mathbf{g}^e$ are the errors of \mathbf{v}^e and \mathbf{g}^e , respectively. $\boldsymbol{\omega}_{ie}^e$, assumed as a constant, is the Earth rotation rate in the ECEF frame. For the low-cost INS, $\delta \mathbf{g}^e$ can be treated as noise. Hence, only $\delta \mathbf{f}^e$ is the nonlinear item in Equation (9). Substitute Equation (1) and $\mathbf{f}^{b'} = \tilde{\mathbf{f}}^{b'} - \delta \mathbf{f}^{b'}$ into Equation (8) and yield:

$$\begin{aligned} \delta \mathbf{f}^{e'} = & \tilde{\mathbf{q}}_b^e \circ \tilde{\mathbf{f}}^{b'} \circ \delta \mathbf{q}_b^{e*} + \delta \mathbf{q}_b^e \circ \tilde{\mathbf{f}}^{b'} \circ \tilde{\mathbf{q}}_b^{e*} + \tilde{\mathbf{q}}_b^e \circ \delta \mathbf{f}^{b'} \circ \tilde{\mathbf{q}}_b^{e*} \\ & - \delta \mathbf{q}_b^e \circ \tilde{\mathbf{f}}^{b'} \circ \delta \mathbf{q}_b^{e*} - \tilde{\mathbf{q}}_b^e \circ \delta \mathbf{f}^{b'} \circ \delta \mathbf{q}_b^{e*} - \delta \mathbf{q}_b^e \circ \delta \mathbf{f}^{b'} \circ \mathbf{q}_b^{e*} + \delta \mathbf{q}_b^e \circ \delta \mathbf{f}^{b'} \circ \delta \mathbf{q}_b^{e*} \end{aligned} \quad (10)$$

If the attitude errors are small enough that the last four items on the right side of Equation (10) can be ignored, Equation (10) can be approximated as:

$$\delta \mathbf{f}^e \approx \tilde{\mathbf{q}}_b^e \circ \tilde{\mathbf{f}}^{b'} \circ \delta \mathbf{q}_b^{e*} + \delta \mathbf{q}_b^e \circ \tilde{\mathbf{f}}^{b'} \circ \tilde{\mathbf{q}}_b^{e*} + \tilde{\mathbf{q}}_b^e \circ \delta \mathbf{f}^{b'} \circ \tilde{\mathbf{q}}_b^{e*} \quad (11)$$

The item, $\delta \mathbf{f}^e$, can be linearized as:

$$\delta \mathbf{f}^e \approx \mathbf{D}^e \delta \mathbf{q}_b^e + \tilde{\mathbf{C}}_b^e \delta \mathbf{f}^{b'} \quad (12)$$

where:

$$\mathbf{u}^e = \begin{bmatrix} u_1^e & u_2^e & u_3^e & u_4^e \end{bmatrix}^T = \tilde{\mathbf{q}}_b^e \circ \tilde{\mathbf{f}}^{b'} \quad (13)$$

$$\mathbf{s}^e = \begin{bmatrix} s_1^e & s_2^e & s_3^e & s_4^e \end{bmatrix}^T = \tilde{\mathbf{f}}^{b'} \circ \tilde{\mathbf{q}}_b^{e*} \quad (14)$$

$$\mathbf{D}^e = \begin{bmatrix} u_2^e + s_2^e & -u_1^e + s_1^e & u_4^e + s_4^e & -u_3^e - s_3^e \\ u_3^e + s_3^e & -u_4^e + s_4^e & -u_1^e + s_1^e & u_2^e + s_2^e \\ u_4^e + s_4^e & u_3^e + s_3^e & -u_2^e - s_2^e & -u_1^e + s_1^e \end{bmatrix} \quad (15)$$

Substitute Equation (12) into Equation (9) and yield:

$$\delta \dot{\mathbf{v}}^e \approx \mathbf{D}^e \delta \mathbf{q}_b^e - 2\omega_{ie}^e \times \delta \mathbf{v}^e + \tilde{\mathbf{C}}_b^e \delta \mathbf{f}^{b'} + \delta \mathbf{g}^e \quad (16)$$

Equation (16) is the linearized velocity error equation using the AQE model in the ECEF frame, but it is derived under small attitude errors. In Equation (10), $\delta \mathbf{f}^{b'}$ is related to the accelerometer errors so the values of $\delta \mathbf{f}^{b'}$ are usually far less than those of $\tilde{\mathbf{f}}^{b'}$. The values of $\delta \mathbf{q}_b^e$ are also far less than those of $\tilde{\mathbf{q}}_b^e$ under small attitude errors. However, with large attitude errors, the values of $\delta \mathbf{q}_b^e$ are no less than those of $\tilde{\mathbf{q}}_b^e$, so the linearized errors would be very large if the four items related to $\delta \mathbf{q}_b^e$ are ignored on the right side of Equation (10). Hence, Equation (16) is only applicable for small attitude errors (i.e., the fine stage of the alignment).

However, in the coarse stage of alignment, although the values of $\delta \mathbf{f}^{b'}$ are still small, the values of $\delta \mathbf{q}_b^e$ are large in Equation (10) because the attitude errors are very large. Hence, the fourth item on the right side of Equation (10) should be taken into account in the linearized equation while the four items related to $\delta \mathbf{f}^{b'}$ can be ignored. That is, $\delta \mathbf{f}^e$ can be approximated as:

$$\delta \mathbf{f}^e \approx (\mathbf{D}^e - \mathbf{E}^e) \delta \mathbf{q}_b^e \quad (17)$$

where:

$$\mathbf{a}^e = \begin{bmatrix} a_1^e & a_2^e & a_3^e & a_4^e \end{bmatrix}^T = \delta \tilde{\mathbf{q}}_b^e \circ \tilde{\mathbf{f}}^{b'} \quad (18)$$

$$\mathbf{b}^e = \begin{bmatrix} b_1^e & b_2^e & b_3^e & b_4^e \end{bmatrix}^T = \tilde{\mathbf{f}}^{b'} \circ \delta \tilde{\mathbf{q}}_b^{e*} \quad (19)$$

$$\mathbf{E}^e = \begin{bmatrix} a_2^e + b_2^e & -a_1^e + b_1^e & a_4^e + b_4^e & -a_3^e - b_3^e \\ a_3^e + b_3^e & -a_4^e + b_4^e & -a_1^e + b_1^e & a_2^e + b_2^e \\ a_4^e + b_4^e & a_3^e + b_3^e & -a_2^e - b_2^e & -a_1^e + b_1^e \end{bmatrix} \quad (20)$$

where $\delta\hat{\mathbf{q}}_b^e$ is the estimated $\delta\mathbf{q}_b^e$. Substitute Equation (17) into Equation (9) and yield:

$$\delta\dot{\mathbf{v}}^e \approx (\mathbf{D}^e - \mathbf{E}^e) \delta\mathbf{q}_b^e - 2\boldsymbol{\omega}_{ie}^e \times \delta\mathbf{v}^e + \delta\mathbf{g}^e \quad (21)$$

Equation (21) is the linearized velocity error equation using the AQE model in the ECEF frame for the coarse stage. It should be noted that the estimated $\delta\mathbf{q}_b^e$, $\delta\hat{\mathbf{q}}_b^e$, is used in Equation (21). Hence, the impact of large errors due to linearized and ignored items in the filtering should be considered in the coarse stage, which will be further addressed in Section 3.

2.3 | Position Error Equations

The position equation in the ECEF frame is as follows:

$$\dot{\mathbf{r}}^e = \mathbf{v}^e \quad (22)$$

where \mathbf{r}^e is the position vector in the ECEF frame. If the position error is denoted as $\delta\mathbf{r}^e = \tilde{\mathbf{r}}^e - \mathbf{r}^e$, there is:

$$\delta\dot{\mathbf{r}}^e = \delta\mathbf{v}^e \quad (23)$$

Equation (23) is the position error equation in the ECEF frame, which is linear.

2.4 | State Equations

If the states are denoted as:

$$\mathbf{x}^e = \left[\delta\mathbf{q}_b^{eT} \quad \delta\mathbf{v}^{eT} \quad \delta\mathbf{r}^{eT} \quad \mathbf{b}_a^T \quad \mathbf{b}_g^T \right]^T \quad (24)$$

herein, the errors of accelerometers and gyroscopes are modeled as:

$$\delta\mathbf{f}^b = \mathbf{b}_a + \mathbf{n}_{ra} \quad (25)$$

$$\delta\boldsymbol{\omega}_{ib}^b = \mathbf{b}_g + \mathbf{n}_{rg} \quad (26)$$

$$\dot{\mathbf{b}}_a = \mathbf{n}_a \quad (27)$$

$$\dot{\mathbf{b}}_g = \mathbf{n}_g \quad (28)$$

where \mathbf{n}_{ra} , \mathbf{n}_{rg} , \mathbf{n}_a , and \mathbf{n}_g are zero-mean white noise.

The state equations include Equations (2), (9), (23), (27), and (28). Because all the equations except Equation (9) are linear, the state equations are linear, too, if the linearized velocity error equations in Equation (16) or (21) are employed. The state equations can be written as:

$$\dot{\mathbf{x}}^e = \mathbf{F}^e \mathbf{x}^e + \mathbf{w}^e \quad (29)$$

In the coarse stage:

$$\mathbf{F}^e = \begin{bmatrix} \mathbf{M}^e & \mathbf{0}_{4 \times 3} & \mathbf{0}_{4 \times 3} & \mathbf{0}_{4 \times 3} & \frac{1}{2} \mathbf{U}^e \\ (\mathbf{D}^e - \mathbf{E}^e) & -2\boldsymbol{\omega}_{ie}^e \times & \mathbf{0}_{3 \times 3} & \mathbf{0}_{3 \times 3} & \mathbf{0}_{3 \times 3} \\ \mathbf{0}_{3 \times 4} & \mathbf{I}_{3 \times 3} & \mathbf{0}_{3 \times 3} & \mathbf{0}_{3 \times 3} & \mathbf{0}_{3 \times 3} \\ \mathbf{0}_{3 \times 4} & \mathbf{0}_{3 \times 3} & \mathbf{0}_{3 \times 3} & \mathbf{0}_{3 \times 3} & \mathbf{0}_{3 \times 3} \\ \mathbf{0}_{3 \times 4} & \mathbf{0}_{3 \times 3} & \mathbf{0}_{3 \times 3} & \mathbf{0}_{3 \times 3} & \mathbf{0}_{3 \times 3} \end{bmatrix} \quad (30)$$

$$\mathbf{w}^e = \begin{bmatrix} \frac{1}{2} \mathbf{U}^e \mathbf{n}_{rg} \\ \delta \mathbf{g}^e \\ \mathbf{0}_{3 \times 1} \\ \mathbf{n}_a \\ \mathbf{n}_g \end{bmatrix} \quad (31)$$

where $\mathbf{I}_{n \times n}$ is an $n \times n$ unit matrix. In the fine stage:

$$\mathbf{F}^e = \begin{bmatrix} \mathbf{M}^e & \mathbf{0}_{4 \times 3} & \mathbf{0}_{4 \times 3} & \mathbf{0}_{4 \times 3} & \frac{1}{2} \mathbf{U}^e \\ \mathbf{D}^e & -2\boldsymbol{\omega}_{ie}^e \times & \mathbf{0}_{3 \times 3} & \tilde{\mathbf{C}}_b^e & \mathbf{0}_{3 \times 3} \\ \mathbf{0}_{3 \times 4} & \mathbf{I}_{3 \times 3} & \mathbf{0}_{3 \times 3} & \mathbf{0}_{3 \times 3} & \mathbf{0}_{3 \times 3} \\ \mathbf{0}_{3 \times 4} & \mathbf{0}_{3 \times 3} & \mathbf{0}_{3 \times 3} & \mathbf{0}_{3 \times 3} & \mathbf{0}_{3 \times 3} \\ \mathbf{0}_{3 \times 4} & \mathbf{0}_{3 \times 3} & \mathbf{0}_{3 \times 3} & \mathbf{0}_{3 \times 3} & \mathbf{0}_{3 \times 3} \end{bmatrix} \quad (32)$$

$$\mathbf{w}^e = \begin{bmatrix} \frac{1}{2} \mathbf{U}^e \mathbf{n}_{rg} \\ \tilde{\mathbf{C}}_b^e \mathbf{n}_{ra} + \delta \mathbf{g}^e \\ \mathbf{0}_{3 \times 1} \\ \mathbf{n}_a \\ \mathbf{n}_g \end{bmatrix} \quad (33)$$

In this paper, the estimated \mathbf{b}_a and \mathbf{b}_g values are only used to compensate for the accelerometer and gyroscope biases in the fine stage since they are not accurate enough for the coarse stage.

2.5 | Measurement Equations

The measurements are the difference between the velocity and position provided by GPS and those output by the INS. The measurement equations are as follows:

$$\mathbf{z}^e = \begin{bmatrix} \mathbf{r}_{GPS}^e \\ \mathbf{v}_{GPS}^e \end{bmatrix} - \begin{bmatrix} \mathbf{r}_{INS}^e \\ \mathbf{v}_{INS}^e \end{bmatrix} = \mathbf{H}^e \mathbf{x}^e + \mathbf{n}^e \quad (34)$$

where $\mathbf{H}^e = \begin{bmatrix} \mathbf{0}_{3 \times 4} & \mathbf{0}_{3 \times 3} & -\mathbf{I}_{3 \times 3} & \mathbf{0}_{3 \times 3} & \mathbf{0}_{3 \times 3} \\ \mathbf{0}_{3 \times 4} & -\mathbf{I}_{3 \times 3} & \mathbf{0}_{3 \times 3} & \mathbf{0}_{3 \times 3} & \mathbf{0}_{3 \times 3} \end{bmatrix}$ and measurement noise, $\mathbf{n}^e = \begin{bmatrix} \delta \mathbf{r}_{GPS}^e \\ \delta \mathbf{v}_{GPS}^e \end{bmatrix}$. The measurement equations in Equation (34) are also linear.

3 | FILTERING

According to the derivation above, the linearized velocity error equations in Equations (16) and (21) are applicable to the fine and coarse stages of alignment, respectively, so that the standard KF can be employed. However, the linearized errors in Equation (21) will be very large in the coarse stage so the linear KF runs the risk of becoming significantly degraded or even diverged.

The most effective method to mitigate the impact of large linearized errors is the use of a fading KF which relies more on the latest measurements than the earlier ones in filtering. The STF algorithm may be more effective than the fading KF in mitigating the linearized error since it adaptively adjusts the fading factor to the residuals in real time.

However, both the fading KF and STF methods may not achieve the desirable results in the coarse alignment because only velocity error equations are linearized (whereas the others are linear). Hence, an improved STF algorithm is proposed to address the difference among the state equations herein.

3.1 | Discrete State and Measurement Equations

If the superscript e is omitted in Equations (29) and (34) for brevity, the state and measurement equations in Equations (29) and (34) can be rewritten as:

$$\dot{\mathbf{x}} = \mathbf{F}\mathbf{x} + \mathbf{w} \quad (35)$$

$$\mathbf{z} = \mathbf{H}\mathbf{x} + \mathbf{n} \quad (36)$$

The corresponding discrete equations can be derived as:

$$\mathbf{x}_k = \Phi_{k-1}\mathbf{x}_{k-1} + \mathbf{w}_{k-1} \quad (37)$$

$$\mathbf{z}_k = \mathbf{H}_k\mathbf{x}_k + \mathbf{n}_k \quad (38)$$

where \mathbf{x}_k is the state vector at time t_k ; Φ_{k-1} is the state transition matrix from t_{k-1} to t_k ; \mathbf{w}_{k-1} is the state noise vector; \mathbf{z}_k is the measurement vector; \mathbf{H}_k is the measurement matrix; \mathbf{n}_k is the measurement error; $E(\mathbf{w}_k) = \mathbf{0}_{16 \times 1}$; $E(\mathbf{n}_k) = \mathbf{0}_{6 \times 1}$; $E(\mathbf{w}_k \mathbf{w}_l^T) = \mathbf{Q}_k \delta_{kl}$; $E(\mathbf{n}_k \mathbf{n}_l^T) = \mathbf{R}_k \delta_{kl}$; $E(\mathbf{x})$ is the expectation of \mathbf{x} ; δ_{kl} is the Kronecker delta function; and \mathbf{Q}_k and \mathbf{R}_k are the covariance matrices of \mathbf{w}_k and \mathbf{n}_k , respectively. Since the updating period, T , is very short (such as 10 ms), Φ_{k-1} is approximated as $(\mathbf{I} + \mathbf{F}T)$.

If there are no errors in both Equations (37) and (38), the standard KF method can achieve the optimal state estimation in the merit of minimum variance. On the contrary, the standard KF will be significantly degraded in performance or even divergent if there are large errors in Equation (37) and/or Equation (38). Hence, a standard KF is usually employed in the fine stage while a more robust algorithm should be used in the coarse stage.

3.2 | Improved STF Algorithm

The improved STF algorithm is composed of two steps, updating and prediction, which is similar to the standard KF algorithm. Equations (39) through (43) explain further.

Updating Step:

$$\mathbf{K}_k = \mathbf{P}_k(-) \mathbf{H}_k^T [\mathbf{H}_k \mathbf{P}_k(-) \mathbf{H}_k^T + \mathbf{R}_k]^{-1} \quad (39)$$

$$\hat{\mathbf{x}}_k(+) = \hat{\mathbf{x}}_k(-) + \mathbf{K}_k [\mathbf{z}_k - \mathbf{H}_k \hat{\mathbf{x}}_k(-)] \quad (40)$$

$$\mathbf{P}_k(+) = (\mathbf{I} - \mathbf{K}_k \mathbf{H}_k) \mathbf{P}_k(-) \quad (41)$$

Prediction Step:

$$\hat{\mathbf{x}}_k(-) = \Phi_{k-1} \hat{\mathbf{x}}_{k-1}(+) \quad (42)$$

$$\mathbf{P}_k(-) = \mathbf{P}_k^{\text{Pos}} + \mathbf{P}_k^{\text{Vel}} + \mathbf{Q}_{k-1} \quad (43)$$

where $\hat{\mathbf{x}}_k$ is the estimate of \mathbf{x}_k ; $(-)$ and $(+)$ denote the values before and after the measurement update, respectively; \mathbf{P}_k is the state error covariance matrix; $\mathbf{P}_k^{\text{Pos}}$ and $\mathbf{P}_k^{\text{Vel}}$ are the two matrices determined by the position and velocity measurements in real time, respectively; and \mathbf{K}_k is the gain matrix.

Obviously, for the standard KF algorithm, $\mathbf{P}_k(-)$ is determined as:

$$\mathbf{P}_k(-) = \Phi_{k-1} \mathbf{P}_{k-1}(+) \Phi_{k-1}^T + \mathbf{Q}_{k-1} \quad (44)$$

For the fading KF algorithm, $\mathbf{P}_k(-)$ is modified as:

$$\mathbf{P}_k(-) = s \Phi_{k-1} \mathbf{P}_{k-1}(+) \Phi_{k-1}^T + \mathbf{Q}_{k-1} \quad (45)$$

where s is the fading factor and $s > 1$. The value of s is usually preset as a constant so the fading KF cannot achieve a better performance by adaptively adjusting the value of s in real time. Hence, in the STF algorithm, s is updated to be:

$$s = \max \left\{ 1, \frac{\text{trace}(\mathbf{L}_k)}{\text{trace}(\mathbf{N}_k)} \right\} \quad (46)$$

where $\max(a, b)$ equals a if $a \geq b$ or b otherwise; $\text{trace}(\mathbf{A})$ is the trace of \mathbf{A} ; and:

$$\tilde{\mathbf{z}}_k = \mathbf{z}_k - \mathbf{H}_k \hat{\mathbf{x}}_k(-) \quad (47)$$

$$\mathbf{C}_k = \frac{\rho \mathbf{C}_{k-1} + \tilde{\mathbf{z}}_k \tilde{\mathbf{z}}_k^T}{1 + \rho} \quad (48)$$

$$\mathbf{L}_k = \mathbf{C}_k - \mathbf{H}_k \mathbf{Q}_k \mathbf{H}_k^T - \mathbf{R}_k \quad (49)$$

$$\mathbf{N}_k = \mathbf{H}_k \Phi_k \mathbf{P}_{k-1}(+) \Phi_k^T \mathbf{H}_k^T \quad (50)$$

where ρ is a constant less than 1 and $\mathbf{C}_1 = \tilde{\mathbf{z}}_1 \tilde{\mathbf{z}}_1^T$.

Hence, both the fading KF and STF algorithms enlarge $\mathbf{P}_k(-)$ with the same scale for all states as shown in Equation (45). However, only the velocity error in the state equations have large linearization errors in the coarse stage, so only parts of $\mathbf{P}_k(-)$ will be affected by linearization errors. Hence, it is more reasonable to fade the parts of $\mathbf{P}_k(-)$ that is more significantly affected by linearization errors than the others. As shown in Equation (43), the velocity-related parts of $\mathbf{P}_k(-)$, $\mathbf{P}_k^{\text{Vel}}$, are faded further in the improved STF algorithm. Both $\mathbf{P}_k^{\text{Pos}}$ and $\mathbf{P}_k^{\text{Vel}}$ are determined as follows.

In Equation (9), only $\delta \mathbf{f}^e$ has large linearized errors, so the state matrix error can be specified as:

$$\tilde{\mathbf{F}} = \mathbf{F} + \Delta \mathbf{F} \quad (51)$$

$$\Delta \mathbf{F} = \begin{bmatrix} \mathbf{0}_{4 \times 4} & \mathbf{0}_{4 \times 3} & \mathbf{0}_{4 \times 3} & \mathbf{0}_{4 \times 3} & \mathbf{0}_{4 \times 3} \\ \Delta \mathbf{F}_{21} & \mathbf{0}_{3 \times 3} & \mathbf{0}_{3 \times 3} & \mathbf{0}_{3 \times 3} & \mathbf{0}_{3 \times 3} \\ \mathbf{0}_{3 \times 4} & \mathbf{0}_{3 \times 3} & \mathbf{0}_{3 \times 3} & \mathbf{0}_{3 \times 3} & \mathbf{0}_{3 \times 3} \\ \mathbf{0}_{3 \times 4} & \mathbf{0}_{3 \times 3} & \mathbf{0}_{3 \times 3} & \mathbf{0}_{3 \times 3} & \mathbf{0}_{3 \times 3} \\ \mathbf{0}_{3 \times 4} & \mathbf{0}_{3 \times 3} & \mathbf{0}_{3 \times 3} & \mathbf{0}_{3 \times 3} & \mathbf{0}_{3 \times 3} \end{bmatrix} \quad (52)$$

where $\tilde{\mathbf{F}}$ and \mathbf{F} are the state matrix with error and the linearized state matrix, respectively, and $\Delta \mathbf{F}$ is the error matrix. Since Φ_{k-1} is approximated as $(\mathbf{I} + \mathbf{F}T)$, the error of Φ_{k-1} can be derived as:

$$\Delta \Phi = \begin{bmatrix} \mathbf{0}_{4 \times 4} & \mathbf{0}_{4 \times 3} & \mathbf{0}_{4 \times 3} & \mathbf{0}_{4 \times 3} & \mathbf{0}_{4 \times 3} \\ \Delta \Phi_{21} & \mathbf{0}_{3 \times 3} & \mathbf{0}_{3 \times 3} & \mathbf{0}_{3 \times 3} & \mathbf{0}_{3 \times 3} \\ \mathbf{0}_{3 \times 4} & \mathbf{0}_{3 \times 3} & \mathbf{0}_{3 \times 3} & \mathbf{0}_{3 \times 3} & \mathbf{0}_{3 \times 3} \\ \mathbf{0}_{3 \times 4} & \mathbf{0}_{3 \times 3} & \mathbf{0}_{3 \times 3} & \mathbf{0}_{3 \times 3} & \mathbf{0}_{3 \times 3} \\ \mathbf{0}_{3 \times 4} & \mathbf{0}_{3 \times 3} & \mathbf{0}_{3 \times 3} & \mathbf{0}_{3 \times 3} & \mathbf{0}_{3 \times 3} \end{bmatrix} \quad (53)$$

The matrix $\mathbf{P}_k(-)$, due to the impact of $\Delta \Phi$, can be written as:

$$\tilde{\mathbf{P}}_k(-) = (\Phi_{k-1} + \Delta \Phi) \mathbf{P}_{k-1}(+) (\Phi_{k-1} + \Delta \Phi)^T + \mathbf{Q}_{k-1} \quad (54)$$

If we let $\Delta \mathbf{P}_k(-) = \tilde{\mathbf{P}}_k(-) - \mathbf{P}_k(-)$, there is:

$$\Delta \mathbf{P}_k(-) = \Phi_{k-1} \mathbf{P}_{k-1}(+) \Delta \Phi^T + \Delta \Phi \mathbf{P}_{k-1}(+) \Phi_{k-1}^T + \Delta \Phi \mathbf{P}_{k-1}(+) \Delta \Phi^T \quad (55)$$

Substituting Equation (53) into Equation (55) yields:

$$\Delta \mathbf{P}_k(-) = \begin{bmatrix} \mathbf{0}_{4 \times 4} & \Delta \mathbf{P}_{12} & \mathbf{0}_{4 \times 3} & \mathbf{0}_{4 \times 3} & \mathbf{0}_{4 \times 3} \\ \Delta \mathbf{P}_{21} & \Delta \mathbf{P}_{22} & \Delta \mathbf{P}_{23} & \Delta \mathbf{P}_{24} & \Delta \mathbf{P}_{25} \\ \mathbf{0}_{3 \times 4} & \Delta \mathbf{P}_{32} & \mathbf{0}_{3 \times 3} & \mathbf{0}_{3 \times 3} & \mathbf{0}_{3 \times 3} \\ \mathbf{0}_{3 \times 4} & \Delta \mathbf{P}_{42} & \mathbf{0}_{3 \times 3} & \mathbf{0}_{3 \times 3} & \mathbf{0}_{3 \times 3} \\ \mathbf{0}_{3 \times 4} & \Delta \mathbf{P}_{52} & \mathbf{0}_{3 \times 3} & \mathbf{0}_{3 \times 3} & \mathbf{0}_{3 \times 3} \end{bmatrix} \quad (56)$$

According to Equation (56), only parts of $\mathbf{P}_k(-)$ are affected by $\Delta \mathbf{F}$. In Equation (56), $\Delta \mathbf{P}_{12}$, $\Delta \mathbf{P}_{32}$, $\Delta \mathbf{P}_{42}$, and $\Delta \mathbf{P}_{52}$ are determined by the first item on the right side of Equation (55). Similarly, $\Delta \mathbf{P}_{21}$, $\Delta \mathbf{P}_{23}$, $\Delta \mathbf{P}_{24}$, and $\Delta \mathbf{P}_{25}$ are determined

by the second item on the right side of Equation (55). However, $\Delta\mathbf{P}_{22}$ is contributed by all three items on the right side of Equation (55).

Substituting Equation (55) into Equation (54) yields:

$$\tilde{\mathbf{P}}_k(-) = \Phi_{k-1} \mathbf{P}_{k-1}(+) \Phi_{k-1}^T + \Delta\mathbf{P}_k(-) + \mathbf{Q}_{k-1} \quad (57)$$

In the fading KF or the STF algorithm, only the first item on the right side of Equation (57) is faded. Herein, the second item on the right side of Equation (57) is also taken into account. Hence, $\mathbf{P}_k(-)$ is modified as Equation (43), where:

$$\mathbf{L}_k = \mathbf{C}_k - \mathbf{H}_k \mathbf{Q}_k \mathbf{H}_k^T - \mathbf{R}_k = \begin{bmatrix} \mathbf{L}_k^{\text{Pos}} & \mathbf{L}_{k,12} \\ \mathbf{L}_{k,21} & \mathbf{L}_k^{\text{Vel}} \end{bmatrix} \quad (58)$$

$$\mathbf{N}_k = \mathbf{H}_k \Phi_k \mathbf{P}_{k-1}(+) \Phi_k^T \mathbf{H}_k^T = \begin{bmatrix} \mathbf{N}_k^{\text{Pos}} & \mathbf{N}_{k,12} \\ \mathbf{N}_{k,21} & \mathbf{N}_{k,22} \end{bmatrix} \quad (59)$$

$$s^{\text{Pos}} = \max \left\{ 1, \frac{\text{trace}(\mathbf{L}_k^{\text{Pos}})}{\text{trace}(\mathbf{N}_k^{\text{Pos}})} \right\} \quad (60)$$

$$\mathbf{P}_k^{\text{Pos}} = s^{\text{Pos}} \Phi_{k-1} \mathbf{P}_{k-1}(+) \Phi_{k-1}^T \quad (61)$$

$$\mathbf{N}'_k = \mathbf{H}_k \Phi_k (\lambda \mathbf{P}_k^{\text{Pos}}) \Phi_k^T \mathbf{H}_k^T = \begin{bmatrix} \mathbf{N}'_{k,11} & \mathbf{N}'_{k,12} \\ \mathbf{N}'_{k,21} & \mathbf{N}'_k^{\text{Vel}} \end{bmatrix} \quad (62)$$

$$s^{\text{Vel}} = \frac{1}{3} \max \left\{ 1, \frac{\text{trace}(\mathbf{L}_k^{\text{Vel}})}{\text{trace}(\mathbf{N}'_k^{\text{Vel}})} \right\} + \frac{2}{3} \quad (63)$$

$$\mathbf{P}_k^{\text{Vel}} = \begin{bmatrix} \mathbf{0}_{4 \times 4} & s^{\text{Vel}} \mathbf{P}_{k,12}^{\text{Pos}} & \mathbf{0}_{4 \times 3} & \mathbf{0}_{4 \times 3} & \mathbf{0}_{4 \times 3} \\ s^{\text{Vel}} \mathbf{P}_{k,21}^{\text{Pos}} & (3s^{\text{Vel}} - 2) \mathbf{P}_{k,22}^{\text{Pos}} & s^{\text{Vel}} \mathbf{P}_{k,23}^{\text{Pos}} & s^{\text{Vel}} \mathbf{P}_{k,24}^{\text{Pos}} & s^{\text{Vel}} \mathbf{P}_{k,25}^{\text{Pos}} \\ \mathbf{0}_{3 \times 4} & s^{\text{Vel}} \mathbf{P}_{k,32}^{\text{Pos}} & \mathbf{0}_{3 \times 3} & \mathbf{0}_{3 \times 3} & \mathbf{0}_{3 \times 3} \\ \mathbf{0}_{3 \times 4} & s^{\text{Vel}} \mathbf{P}_{k,42}^{\text{Pos}} & \mathbf{0}_{3 \times 3} & \mathbf{0}_{3 \times 3} & \mathbf{0}_{3 \times 3} \\ \mathbf{0}_{3 \times 4} & s^{\text{Vel}} \mathbf{P}_{k,52}^{\text{Pos}} & \mathbf{0}_{3 \times 3} & \mathbf{0}_{3 \times 3} & \mathbf{0}_{3 \times 3} \end{bmatrix} \quad (64)$$

where λ is a constant and $\lambda = 3$ in the following vehicle test. As expressed in Equation (43), the first two items on the right side are faded by the STF method. The fading factor s^{Pos} is related to the position measurements while s^{Vel} is mainly related to the velocity measurements. Since $\Delta\mathbf{P}_{22}$ is contributed by all three items on the right side of Equation (55), $\mathbf{P}_{k,22}^{\text{Pos}}$ in Equation (64) is multiplied by $(3s^{\text{Vel}} - 2)$.

4 | EXPERIMENTS

The performance of the proposed two-stage alignment in the ECEF frame was verified by two simulations as well as a vehicle test. In both the simulations and the vehicle test, the biases and the random walks of the gyroscopes and accelerometers were $0.1^\circ/\text{s}$, $0.02^\circ/\text{h}^{1/2}$, 16 mg , and $1.3 \times 10^{-4} \text{ m/s}^{3/2}$, respectively. The GPS receiver had a position error of 5 m and a velocity error of 0.2 m/s, respectively.

The GPS receiver's data were sampled at 1 Hz while the IMU data were acquired at 100 Hz.

In the vehicle test, a Unicorecomm UR370 real-time kinematic (RTK) receiver used as a reference had position, velocity, and attitude errors of 0.01 m, 0.03 m/s, and 1° (0.8-m baseline), respectively. The RTK receiver's data were sampled at 1 Hz. The RTK receiver had two antennas so it could measure two attitude angles of the vehicle. In the test, the two antennas were put along the vehicle's body direction so that the yaw and pitch angles of the vehicle could be measured.

The level adjustment was not performed herein. The performance of the alignments are evaluated in the local level frame since the output of the RTK receiver is in the local level frame. The local level frame is herein referred to as the east-north-up (ENU) frame. The initial attitude errors were set as large as $[100^\circ, 100^\circ, 100^\circ]$ in the local level frame to evaluate the performance of the alignments under large initial attitude errors.

The coarse alignments with the fading KF, the STF, and the improved STF algorithms are switched to fine alignments with the standard KF algorithm if the criterion for the transition is satisfied (Wang et al., 2020). In experimentation, it requires the module of the estimated attitude error vector to be less than 5° for 10 s. The coarse alignment with the OBA algorithm switches to a fine alignment with the standard KF algorithm after a preset epoch. Herein, the switch time was set at 50 s.

4.1 | Simulations

A car moving in a plane is simulated herein. In the following two simulations, the trajectories composed of U-turns and lines, which are convenient to implement in applications, are beneficial to improving observability in the alignment since the car's acceleration is changing all the time (Li et al., 2015; Rhee et al., 2004). Figures 1 and 2 depict the trajectory and car velocities in the ENU frame in the first simulation, respectively. The car ran along a figure-8-shaped trajectory for six laps over 288 s.

Figure 3 depicts the yaw errors for the fading KF, original STF, and improved STF algorithms for the coarse stage and the standard KF algorithm for the fine stage in the ECEF frame, respectively. The yaw errors with the OBA algorithm for the coarse stage and the standard KF algorithm for the fine stage in the ECEF frame are also provided in Figure 3 for comparison. The coarse alignments with the fading KF, original STF, and improved STF algorithms were switched to fine alignment with the standard KF algorithm at 124 s, 58 s, and 36 s, respectively. However, the coarse alignment with the OBA algorithm was switched to the fine ones with the standard KF algorithm at 50 s. The converging process of the pitch errors was similar to that of the yaw errors in Figure 3, so it is not provided.

In Figure 3, the yaw errors were very large at the beginning of the coarse stages for the four algorithms, but they converged to small values with the coarse alignments going on. In particular, it took the improved STF algorithm only 36 s to reduce the yaw error from 100° to 5° or less as shown in Figure 3. However, it took the STF algorithm 58 s and the fading KF algorithm 124 s to reduce the yaw error to 5° or less, respectively. Hence, the STF algorithm was faster in converging than the fading KF algorithm, since the fading factor was adjusted adaptively in the former but set as a constant in the latter. Moreover, the improved STF algorithm was even faster in converging than the original STF algorithm due to the specific treatment of the linearized velocity error equation in the improved STF algorithm.

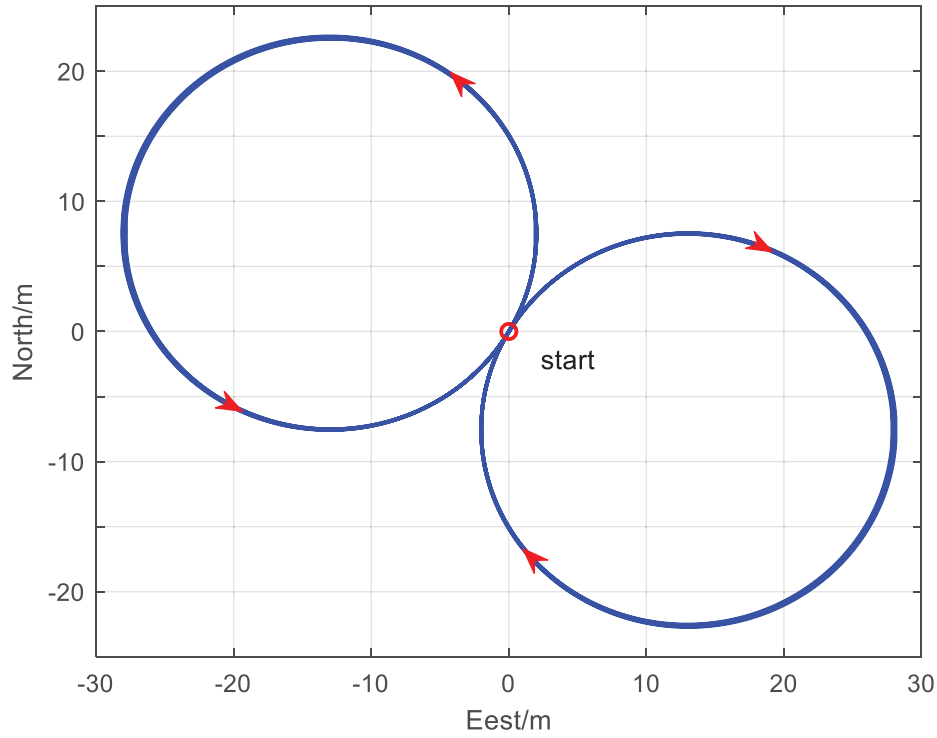


FIGURE 1 The figure-8 trajectory for the first simulation

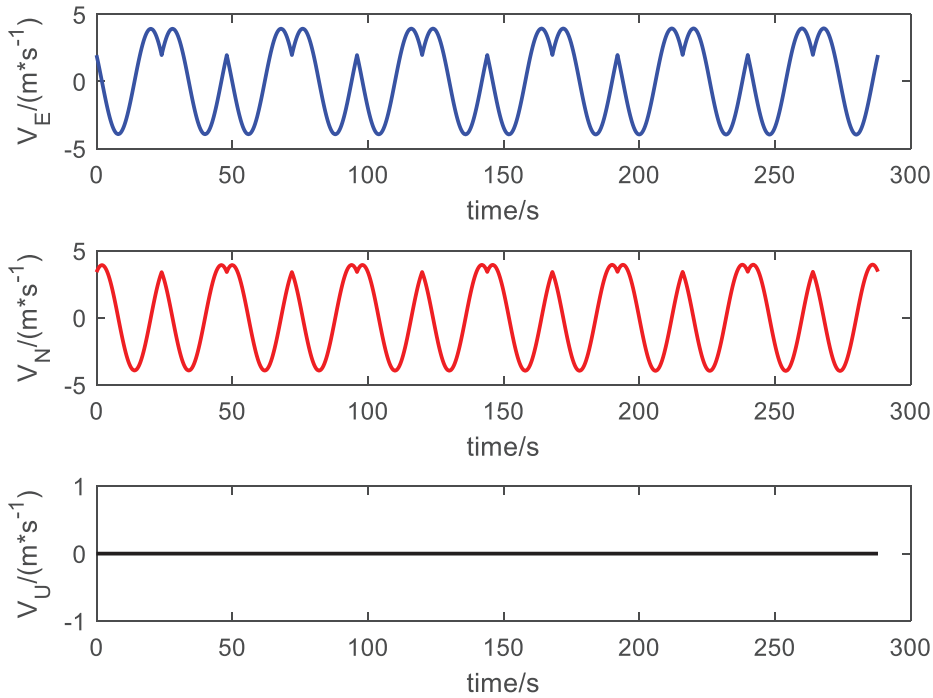


FIGURE 2 The car velocities in the ENU frame in the first simulation

It should be noted that the OBA algorithm converged the fastest of all four algorithms for coarse alignment. It took the OBA algorithm just 20 s to reduce the yaw error to 5° or less. Unfortunately, as mentioned in the introduction, the OBA algorithm in the coarse stage can initialize neither the states nor their covariances

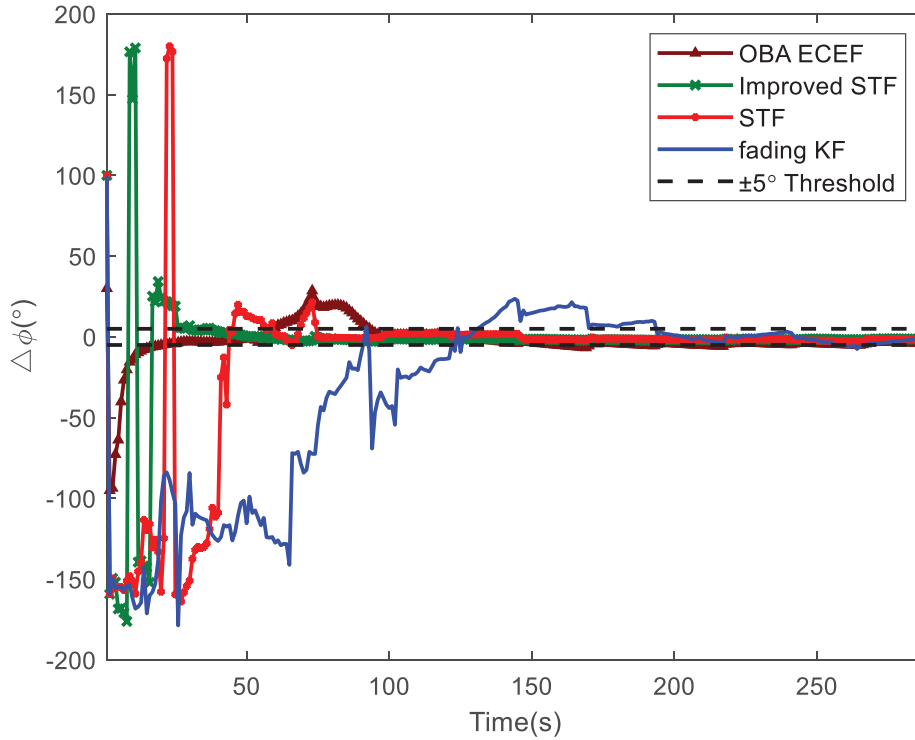


FIGURE 3 Yaw errors for the fading KF, original STF, and improved STF algorithms in the ECEF frame

directly in the following fine stage, which is not good for KF convergence. As illustrated in Figure 3, it took the standard KF algorithm in the fine stage more than 50 s to converge if the OBA algorithm was used in the coarse stage, while it took the standard KF algorithm in the fine stage no more than 5 s to converge if the improved STF algorithm was employed in the coarse stage. Hence, the improved STF algorithm is desirable for the coarse alignment compared with the other three algorithms.

The trajectory and car velocities in the ENU frame in the second simulation are shown in Figures 4 and 5, respectively. The car ran along the long square trajectory for eight laps over 304 s. Obviously, in practice, the long square trajectory in Figure 4 would be easier to implement than the figure-8 trajectory in Figure 1. Figure 6 depicts the yaw errors. As shown in Figure 6, coarse alignments with the fading KF, original STF, and improved STF algorithms were switched to fine ones with the standard KF algorithm at 119 s, 62 s, and 29 s, respectively. The OBA algorithm also converged the fastest of the four algorithms for coarse alignment, but it took the following fine alignment more than 50 s to converge, which was similar to that in Figure 3. That is, the alignments in the second simulation achieved almost the same performance as those in the first simulation, but the long square trajectory would be easier to implement in practice than the figure-8 trajectory. Hence, only the long square trajectory was further employed in the following vehicle test.

4.2 | Vehicle test

The performance of the proposed alignment was further verified by a vehicle test. In the test system shown in Figure 7, there was an ARM® STM32F103 controller

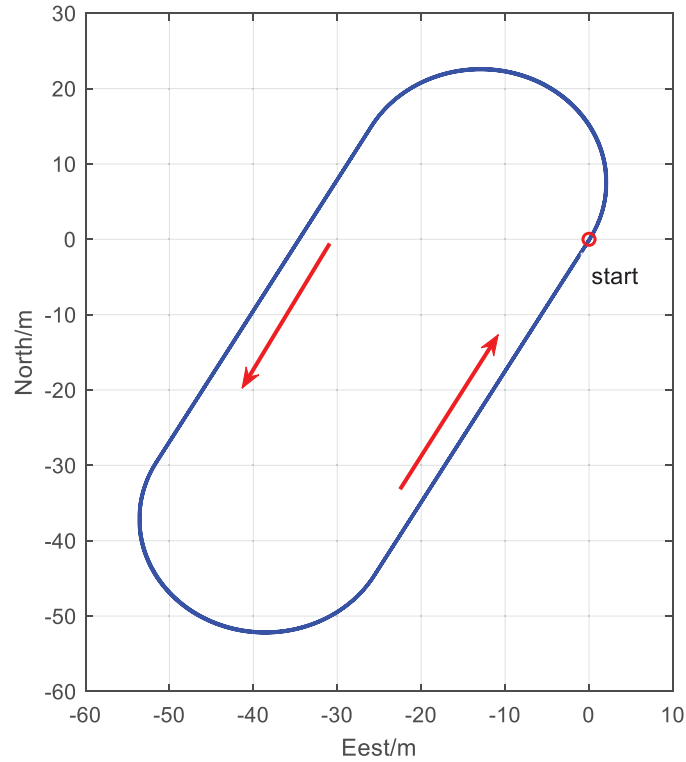


FIGURE 4 The long square trajectory for the second simulation

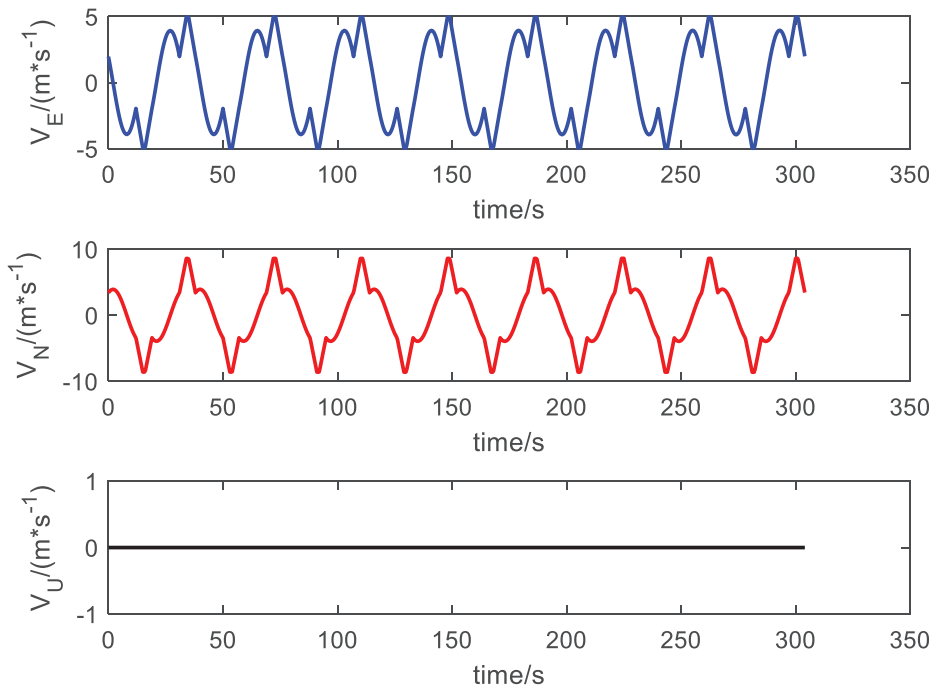


FIGURE 5 Car velocities in the ENU frame in the second simulation

with a frequency of 166 MHz, an AD[®] ADIS16375 MEMS IMU, a u-blox[®] NEO-6M GPS receiver, and a Unicorecomm UR370 RTK receiver. More of the main specifications of the test system are listed at the beginning of the section. The test system

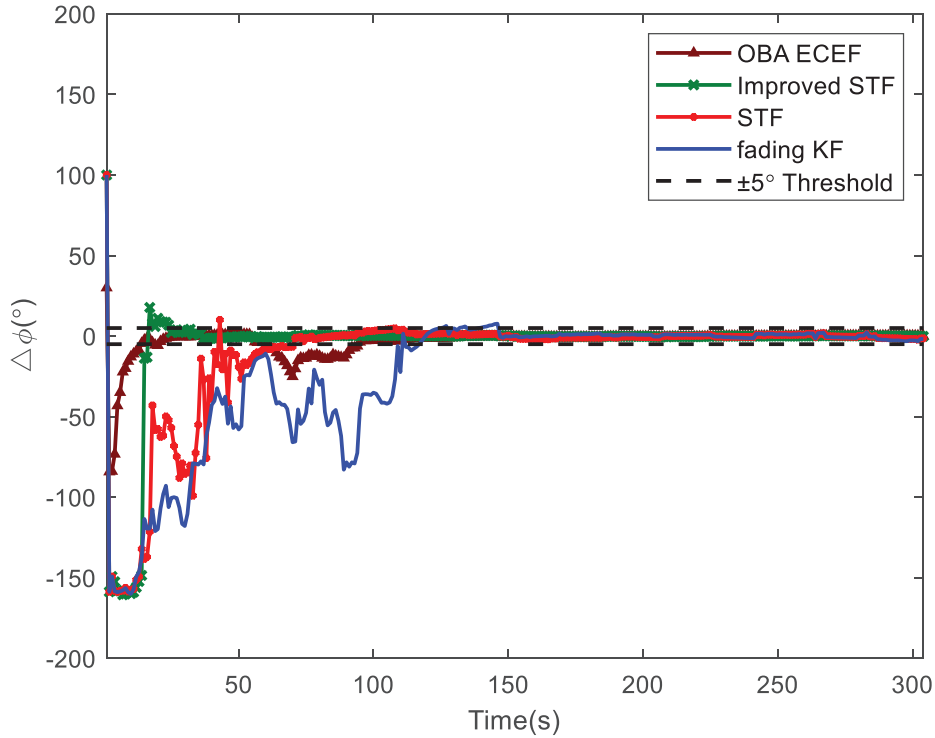


FIGURE 6 Yaw errors for the fading KF, original STF, and improved STF algorithms in the ECEF frame

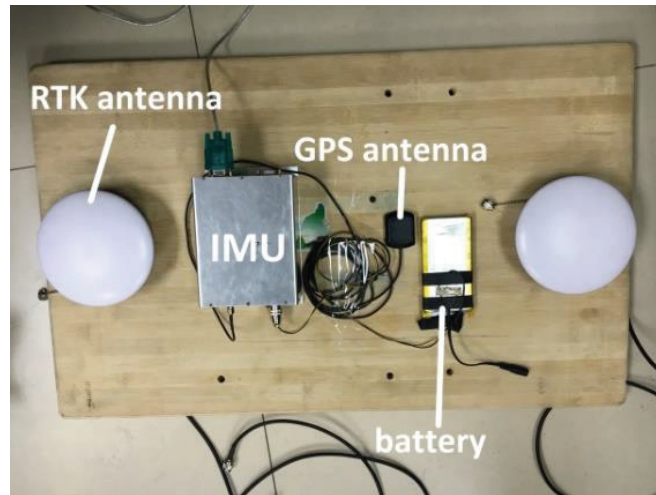


FIGURE 7 Setup of the test system

was mounted on the top of the vehicle in test. The IMU, GPS, and RTK data in the test, which are the same as those in Wang et al. (2020), were sampled and saved for offline processing. As shown in Figure 8, the vehicle ran along a long square trajectory similar to that in Figure 4. Its velocities are depicted in Figure 9. Herein, the outputs of the MEMS IMU and the NEO-6M GPS receiver were used to verify the performance of the alignment algorithms and those of the RTK receiver were used for reference.

Figure 10 depicts yaw errors. As shown in Figure 10, the coarse alignments for the fading KF, original STF, and improved STF algorithms were switched to the

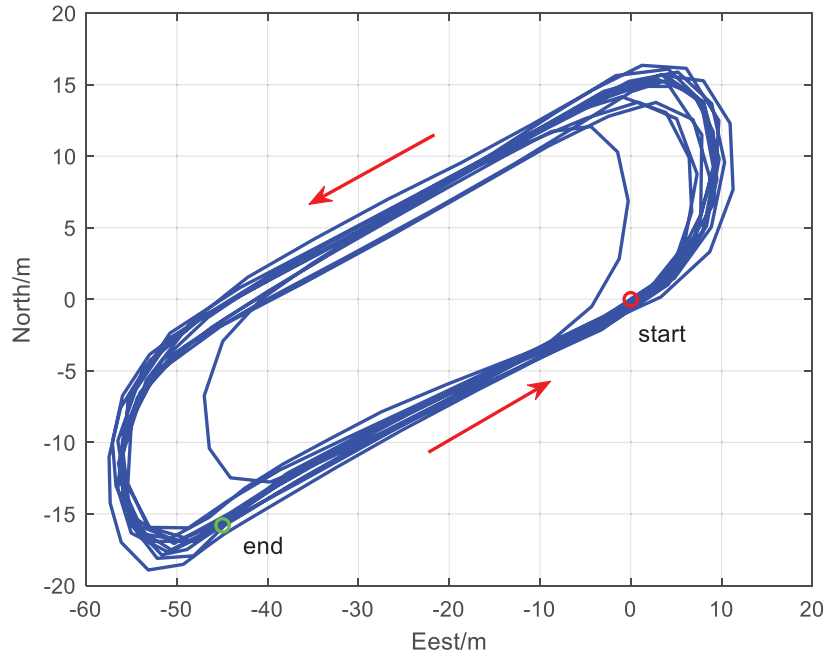


FIGURE 8 The car trajectory in the test

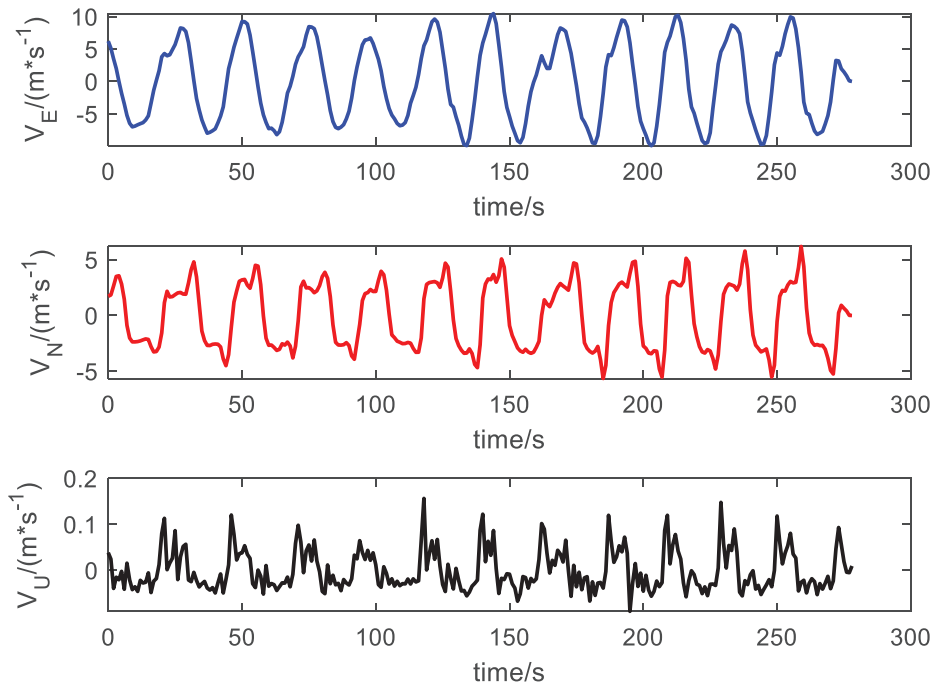


FIGURE 9 The car velocities in the ENU frame in the test

fine ones with the standard KF algorithm at 149 s, 54 s, and 39 s, respectively. The OBA algorithm converged fastest of all four algorithms for coarse alignment once more, but it took the standard KF algorithm in the following fine alignment more than 25 s to converge, which is similar to the results in the previous two simulations. That is, the alignments in the vehicle test had similar performance to those in the two prior simulations.

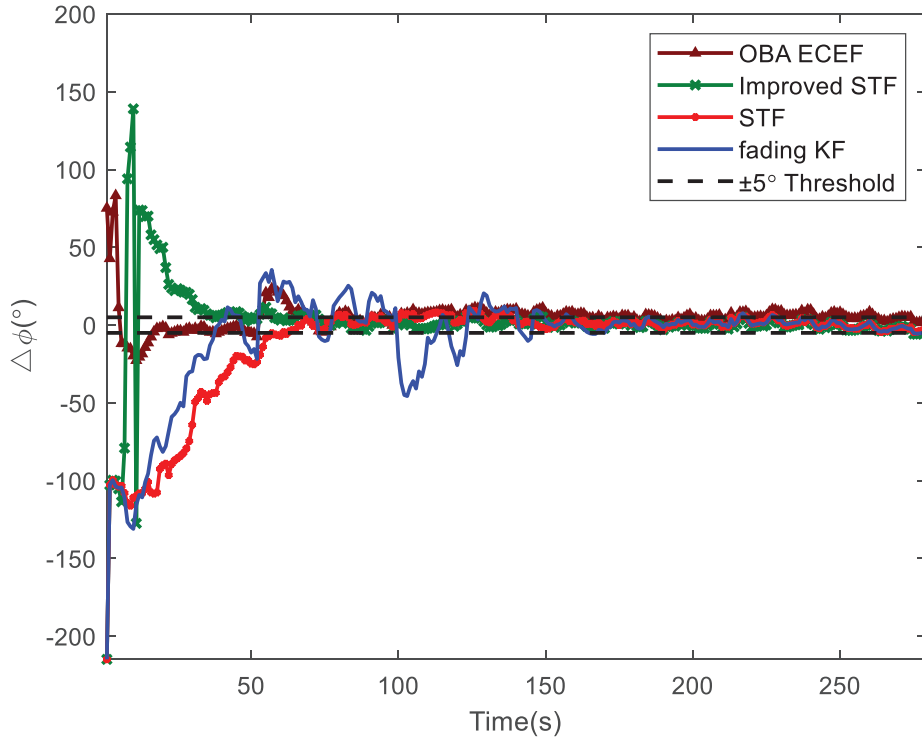


FIGURE 10 Yaw errors for the fading KF, original STF, and improved STF algorithms in the ECEF frame

5 | CONCLUSION

Aiming to provide a fast initial alignment algorithm for a low-cost INS in the ECEF frame under the condition of large initial attitude errors (since the alignment and the following navigation in the ECEF frame is efficient in computation), a two-stage in-motion alignment with GPS measurements was proposed using the AQE model. An improved STF algorithm was proposed for the coarse stage while the standard KF was used for the fine stage. Although the initial attitude errors were very large, level adjustment was not needed for the improved STF algorithm so the time previously reserved for adjustment is no longer necessary.

Both of the simulations as well as the following vehicle test proved that the improved STF algorithm was fastest among the three algorithms for the coarse stage under the same conditions. The main reason for this lies in the specific processing of the linearized velocity error equations in the improved STF algorithm. Although the OBA algorithm converges faster than the improved STF algorithm, the standard KF algorithm in the subsequent fine alignment would take an extra period of time to converge. Hence, the proposed two-stage alignment method is especially appropriate for low-cost INS applications, such as self-driving cars, due to its low computational load and fast convergence.

ACKNOWLEDGMENTS

This paper is sponsored by National Natural Science Foundation under the grant number 62173011.

REFERENCES

- Chang, L., Li, J., & Li, K. (2016). Optimization-based alignment for strapdown inertial navigation system: comparison and extension. *IEEE Transactions on Aerospace and Electronic Systems*, 52(4), 1697–1713. <https://doi.org/10.1109/TAES.2016.130824>
- Chen, Y., Li, W., & Wang, Y. (2021). A robust adaptive indirect in-motion coarse alignment method for GPS/SINS integrated navigation system. *Measurement*, 172, 108834. <https://doi.org/10.1016/j.measurement.2020.108834>
- Dmitriyev, S. P., Stepanov, O. A., & Shepel, S. V. (1997). Nonlinear filtering methods application in INS alignment. *IEEE Transactions on Aerospace and Electronic Systems*, 33(1), 260–272. <https://doi.org/10.1109/7.570762>
- Geng, Y., & Wang, J. (2008). Adaptive estimation of multiple fading factors in Kalman filter for navigation applications. *GPS Solutions*, 12(4), 273–279. <https://doi.org/10.1007/s10291-007-0084-6>
- Han, S., & Wang, J. (2010). A novel initial alignment scheme for low-cost INS aided by GPS for land vehicle applications. *Journal of Navigation*, 63(4), 663–680. <https://doi.org/10.1017/S0373463310000214>
- Kaygisiz, B. H., & Şen, B. (2014). In-motion alignment of a low-cost GPS/INS under large yaw error. *Journal of Navigation*, 68(2), 355–366. <https://doi.org/10.1017/S0373463314000629>
- Kong, X., Nebot, E. M., & Durrant-Whyte, H. (1999). Development of a nonlinear psi-angle model for large misalignment errors and its application in INS alignment and calibration. *Proc. of IEEE International Conference on Robotics and Automation*, Detroit, MI, 1430–1435. <https://doi.org/10.1109/ROBOT.1999.772561>
- Li, W., & Wang, J. (2012). Effective adaptive Kalman filter for MEMS-IMU/magnetometers integrated attitude and yaw reference systems. *Journal of Navigation*, 66(1), 99–113. <https://doi.org/10.1017/S0373463312000331>
- Li, Y., Niu, X., Cheng, Y., Shi, C., & El-Sheimy, N. (2015). The impact of vehicle maneuvers on the attitude estimation of GNSS/INS for mobile mapping. *Journal of Applied Geodesy*, 9(3), 183–197. <https://doi.org/10.1515/jag-2015-0002>
- Pham, T. M. (1991). Kalman filter mechanization for INS airstart. *Proc. of IEEE/AIAA 10th Digital Avionics Systems Conference*, Los Angeles, CA, 516–525. <https://doi.org/10.1109/DASC.1991.177219>
- Qi, N., & Pengfei, Z. (2015). SINS in-motion alignment for initial attitude uncertainty. *Proc. of IEEE 5th International Conference on Instrumentation and Measurement, Computer, Communication and Control*, Qinhuangdao, China, 200–203. <https://doi.org/10.1109/IMCCC.2015.49>
- Rhee, I., Abdel-Hafez, M. F., & Speyer, J. L. (2004). Observability of an integrated GPS/INS during maneuvers. *IEEE Transactions on Aerospace and Electronic Systems*, 40(2), 526–535. <https://doi.org/10.1109/TAES.2004.1310002>
- Rogers, R. M. (1997). IMU in-motion alignment without benefit of attitude initialization. *NAVIGATION*, 44(3), 301–311. <https://doi.org/10.1002/j.2161-4296.1997.tb02349.x>
- Shin, E. -H., & El-Sheimy, N. (2004). An unscented Kalman filter for in-motion alignment of low-cost IMUs. *Proc. of IEEE Position, Location, and Navigation Symposium (PLANS 2004)*, Monterey, CA, 273–279. <https://doi.org/10.1109/PLANS.2004.1309005>
- Simon, D. (2006). *Optimal state estimation: Kalman, H ∞ , and nonlinear approaches*. John Wiley & Sons Inc. <https://doi.org/10.1002/0470045345>
- Syed, Z. F., Aggarwal, P., Niu, X., & El-Sheimy, N. (2008). Civilian vehicle navigation: required alignment of the inertial sensors for acceptable navigation accuracies. *IEEE Transactions on Vehicular Technology*, 57(6), 3402–3412. <https://doi.org/10.1109/TVT.2008.921616>
- Tsukerman, A., & Klein, I. (2018). Analytic evaluation of fine alignment for velocity aided INS. *IEEE Transactions on Aerospace and Electronic Systems*, 54(1), 376–384. <https://doi.org/10.1109/TAES.2017.2760520>
- Wang, K., Xu, X., Gao, W., & Wang, J. (2020). Linearized in-motion alignment for a low-cost INS. *IEEE Transactions on Aerospace and Electronic Systems*, 56(3), 1917–1925. <https://doi.org/10.1109/TAES.2019.2936780>
- Wei, M., & Schwarz, K. P. (1990). A strapdown inertial algorithm using an Earth-fixed Cartesian frame. *NAVIGATION*, 37(2), 153–167. <https://doi.org/10.1002/j.2161-4296.1990.tb01544.x>
- Wu, Y., & Pan, X. (2013). Velocity/position integration formula part I: application to in-flight coarse alignment. *IEEE Transactions on Aerospace and Electronic Systems*, 49(2), 1006–1023. <https://doi.org/10.1109/TAES.2013.6494395>
- Wu, Y., Wang, J., & Hu, D. (2014). A new technique for INS/GNSS attitude and parameter estimation using online optimization. *IEEE Transactions on Signal Processing*, 62(10), 2642–2655. <https://doi.org/10.1109/TSP.2014.2312317>
- Xie, B., Jiang, Y. F., Yan, G. M., & Chen, Y. (2014). Indirect fine-alignment algorithm of in-motion SINS based on ECEF-frame. *Journal of Chinese Inertial Technology*, 22(5), 593–596. <https://doi.org/10.13695/j.cnki.12-1222/o3.2014.05.007>

- Yu, M. -J., Lee, J. G., & Park, H. -W. (1999). Comparison of SDINS in-flight alignment using equivalent error models. *IEEE Transactions on Aerospace and Electronic Systems*, 35(3), 1046–1054. <https://doi.org/10.1109/7.784073>
- Yu, M. -J., Park, H. -W., & Jeon, C. -B. (1997). Equivalent nonlinear error models of strapdown inertial navigation system. *Proc. of Guidance, Navigation, and Control Conference*, New Orleans, LA, 581–587. <https://doi.org/10.2514/6.1997-3563>
- Zhong, M., Guo, J., & Zhou, D. (2018). Adaptive in-flight alignment of INS/GPS systems for aerial mapping. *IEEE Transactions on Aerospace and Electronic Systems*, 54(3), 1184–1196. <https://doi.org/10.1109/TAES.2017.2776058>

How to cite this article: Wang, K., Gao, W., Xu, X., & Wang, J. (2023). Adaptive alignment for low-cost INS in ECEF frame under large initial attitude errors. *NAVIGATION*, 70(1). <https://doi.org/10.33012/navi.554>